Pharm Res (2010) 27:1800–1811
DOI 10.1007/s11095-010-0165-z

RESEARCH PAPER

Evaluation of Enhanced Condensational Growth (ECG) for Controlled Respiratory Drug Delivery in a Mouth-Throat and Upper Tracheobronchial Model

Michael Hindle • P. Worth Longest

Received: 3 March 2010 / Accepted: 21 April 2010 / Published online: 8 May 2010

ABSTRACT

Purpose The objective of this study is to evaluate the effects of enhanced condensational growth (ECG), as a novel inhalation drug delivery method, on nano-aerosol deposition in a mouth-throat (MT) and upper tracheobronchial (TB) model using *in vitro* experiments and computational fluid dynamics (CFD) simulations.

Methods Separate streams of nebulized nano-aerosols and saturated humidified air (39°C—ECG; 25°C—control) were combined as they were introduced into a realistic MT-TB geometry. Aerosol deposition was determined in the MT, generations G0-G2 (trachea—lobar bronchi) and G3-G5 and compared to CFD simulations.

Results Using ECG conditions, deposition of 560 and 900 nm aerosols was low in the MT region of the MT-TB model. Aerosol drug deposition in the G0-G2 and G3-G5 regions increased due to enhanced condensational growth compared to control. CFD-predicted depositions were generally in good agreement with the experimental values.

Conclusions The ECG platform appears to offer an effective method of delivering nano-aerosols through the extrathoracic region, with minimal deposition, to the tracheobronchial airways and beyond. Aerosol deposition is then facilitated as enhanced condensational growth increases particle size. Future studies will investigate the effects of physio-chemical drug properties and realistic inhalation profiles on ECG growth characteristics.

KEY WORDS computational fluid dynamics · condensational growth · *in vitro* aerosol deposition · nano-aerosol drug delivery · respiratory drug delivery

ABBREVIATIONS

CFD	computational fluid dynamics
DPI	dry powder inhaler
ECG	enhanced condensational growth
G	generation
MDI	metered dose inhaler
MT	mouth-throat
SD	standard deviation
TB	tracheobronchial

INTRODUCTION

Despite their widespread use, metered dose inhalers (MDI) and dry powder inhalers (DPI) are recognized as delivering drugs to the lungs with low deposition efficiencies and high variability (1). These devices are characterized as having significant drug deposition in the extrathoracic airways (including the mouth and throat), which reduces the amount of drug available for deposition at the site of action within the lungs (2,3). Perhaps as significant as the low pulmonary drug deposition efficiency, is the large intra- and inter-subject lung deposition variability (1). If the lungs are to be used as a route of administration for envisioned next-generation systemically acting compounds, which may require precise dosing regimens and are more expensive, new delivery platforms will be required (4,5).

M. Hindle (✉) · P. W. Longest
Department of Pharmaceutics, Virginia Commonwealth University
410 N. 12th St.
P.O. Box 980533, Richmond, Virginia 23298-0533 USA
e-mail: mhindle@vcu.edu

P. W. Longest
Department of Mechanical Engineering
Virginia Commonwealth University
Richmond, Virginia, USA

The aerodynamic particle size of the inhalation aerosols generated by MDIs and DPIs is known to be a key determinant of the fate of the drug following aerosol generation. These devices typically generate aerosols with mass median aerodynamic diameters (MMAD) of 2–6 μm (4,6,7). For these aerosols, this size range causes significant deposition in the mouth-throat (MT) and upper tracheobronchial (TB) airways (1,3,6,8). Deposition may be further enhanced by inhaler momentum effects, resulting in up to approximately 50% drug loss in the MT region of the airways and the low and variable pulmonary deposition described earlier (6,9,10). Reducing the aerodynamic particle size of the aerosols may offer a solution to this MT deposition. Nanometer aerosols greater than 10 nm have been observed to effectively penetrate the MT, with particles in the size range of 10–900 nm reported to have deposition efficiencies of less than 5% in the extrathoracic region (11,12).

The pharmaceutical delivery of nano-aerosols to the lungs offers a unique drug delivery opportunity due to the inherent characteristics of the aerosols and the route of administration (13). Nano-aerosols possess a small size with a large surface area, together with altered dissolution properties compared to micrometer-sized particles. The lungs offer a large surface area for absorption and low protease activity, and this route avoids hepatic first-pass metabolism. Nano-aerosol pulmonary delivery offers great potential for the treatment of local lung diseases and for the delivery of drugs to the systemic circulation (13,14). Current applications being investigated include the targeting of nanoparticles to treat lung cancer, respiratory and systemic infections, and gene delivery for the treatment of cystic fibrosis (4,5). However, despite intense research activity, the full potential for nano-aerosol drug delivery has yet to be realized. Nanometer aerosols greater than 10 nm are observed to penetrate the mouth-throat region with high efficiency; however, pulmonary deposition is low, with approximately 70% of the particles exhaled (15–18). This low pulmonary retention is due to the aerosols lacking sufficient mass and inertia to deposit in the lungs.

The present solution employed to deliver nanoparticles to the lungs has been to incorporate them into conventional MDI, DPI or nebulizer formulations. Inhaled nanoparticles have been formulated as suspended particles in nebulized droplets and MDIs, or they are combined with large carrier particles in DPIs (19–22). The primary limitations of these systems include the same drawbacks encountered by the current generation of inhaled pharmaceuticals. Namely, they are often deposited in the lung at very low deposition efficiencies and with high intra- and inter-subject dose variability (1).

It is well known that hygroscopic aerosols increase in size due to water vapor condensation in the warm and humid respiratory airways (23–26). However, the size increase of nano-aerosols at an *in vivo* relative humidity of 99.5% is insufficient to increase lung retention, as evidenced by the significant exhaled fraction. Enhanced condensational growth (ECG) is a newly proposed respiratory drug delivery platform that is intended to provide both low MT deposition and high lung retention of nano-aerosols (27,28). This approach consists of combining nano-aerosols with a source of saturated or supersaturated water vapor during inhalation. Condensation of water vapor onto droplet surfaces causes the nano-aerosol size to increase at a controlled rate (29,30). The intent is for the aerosol to remain nano-sized or submicrometer while in the MT region of the respiratory tract, thereby minimizing deposition and drug loss. As the aerosol enters the lungs, continued growth results in a significant size increase and subsequent deposition due to inertial impaction and sedimentation. The rate of size growth, the final aerosol size, and therefore the deposition site can be controlled by optimizing the nano-aerosol and the ECG conditions. Factors affecting the rate of growth include the initial aerosol size, drug hygroscopicity, and the gas phase conditions of the humidity and aerosol delivery streams (i.e., temperature, relative humidity, and flow rate).

Previous studies have demonstrated the feasibility of the ECG approach in a simple tubular geometry (27). *In vitro* findings indicated that aerosol size increased from the submicrometer range to an ideal target size of 2 to 3 μm, which should ensure full lung retention. This increase in size occurred within approximately 0.2–0.4 s, which is approximately equal to the residence time of an aerosol traveling from the mouth to the first respiratory bifurcation under standard inhalation conditions. Computational fluid dynamics (CFD) simulations of ECG in the tubular system demonstrated steady aerosol size increase over the entire length of the geometry (31). Two-way coupling effects were found to be significant, in which the aerosol number concentration limited the rate of growth. Good agreement was found between the CFD model predictions of outlet aerosol size and the *in vitro* results. However, aerosol deposition was not considered in the simple tubular model. Therefore, it is not known if the aerosol is sufficiently small in the MT region to reduce deposition. Furthermore, growth profiles and deposition in the upper TB region should be considered. As a result, evaluation of the ECG process is needed in a more realistic model of the MT and upper TB geometry, which includes predictions of sectional deposition and aerosol size change.

The objective of this study is to evaluate the performance of the ECG process on nano-aerosol drug deposition in a model of the mouth-throat and upper tracheobronchial (MT-TB) geometry using both *in vitro* experiments and CFD simulations. Inhalation temperatures and initial

particle sizes that minimize MT deposition and provide sufficient growth to ensure lung retention are sought. The *in vitro* experiments will be used to determine deposition within individual sections of the MT-TB model, which include the oropharynx, generations G0 (trachea)–G2 (lobar bronchi), and G3 (segmental bronchi)–G5. The CFD predictions will first be validated with comparisons to the *in vitro* deposition results, on a sectional basis, for multiple initial particle sizes (560 and 900 nm) and inhalation temperature conditions (25 and 39°C). The numerical model will then be used to evaluate the rate of aerosol size increase and the polydisperse final aerosol size. Deposition results will also be compared with a metered dose inhaler in the same MT-TB model to demonstrate the benefits of reducing the particle size. Finally, the CFD model will be applied to consider improved inhalation temperature conditions for further reducing MT deposition and fostering aerosol growth deeper within the respiratory airways.

METHODS

Aerosol Generation Methods

Nano-sized aqueous droplet drug aerosols were generated using a small particle aerosol generator (SPAG-6000, ICN Pharmaceuticals, Costa Mesa, CA). Albuterol sulfate solutions were nebulized and dried using a series of nebulizer airflow conditions to produce aerosols with initial mean MMADs (and standard deviations) of 560 (11.4) nm and 900 (32.7) nm, respectively. The 560 nm aerosol was generated using a 0.1% albuterol sulfate in water solution with a nebulizer gas flow rate of 7.5 L/min and a drying gas flow rate of 3 L/min. The 900 nm aerosol was generated using a 0.5% albuterol sulfate in water solution with a nebulizer gas flow rate of 7 L/min and a drying gas flow rate of 3 L/min. Aerosols were generated for 2.5 and 1.0 min, respectively, for the 560 and 900 nm aerosols. For comparison, an albuterol sulfate MDI (Proventil HFA, Key Pharmaceuticals, Kenilworth, NJ) was actuated (5 doses with an emitted dose of 108 μg per actuation) into the MT-TB geometry, which had an air flow rate of 30 L/min drawn through it.

In Vitro MT-TB Model and Mouthpiece

Fig. 1 shows the physical model of the MT-TB geometry that was used in this study together with the dual flow mouthpiece adapter used to deliver the nebulized drug aerosol and humidified air to the model. A conventional MDI mouthpiece adapter was used to connect the MDI to the mouth inlet of the model. The hollow model of the respiratory tract geometry was generated using an in-house rapid prototyper (Viper SLA, 3D Systems, Valencia, CA). This rapid prototyping machine employs a 100 mW solid-state laser to selectively harden Accura 60 (3D Systems) clear plastic resin. As shown in Fig. 1(a), the MT geometry is based on the elliptical model

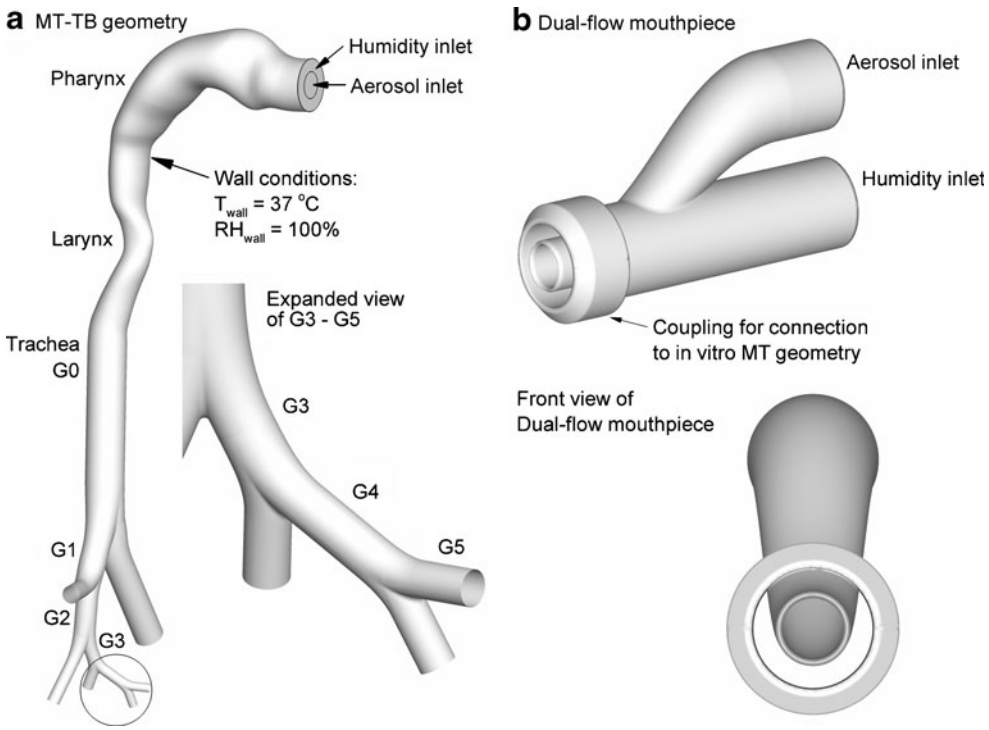

Fig. 1 Geometry used to assess enhanced condensational growth (ECG) consisting of **a** mouth-throat (MT) and tracheobronchial (TB) regions extending down a single path to respiratory generation G5; and **b** a dual-flow mouthpiece.

proposed by Xi and Longest (32). The TB geometry was constructed using idealized branching units, based on the "Physiologically Realistic Bifurcation" (PRB) geometry specified by Heistracher and Hofmann (33). Bifurcations down a "single path" were considered extending from the trachea (G0) to generation 5 (G5) of the right lower lung lobe. Airway model parameters such as branch diameter, length, bifurcation angle, and gravity angle were based on measurements reported by Yeh and Schum (34). As illustrated in Fig. 1, the model is asymmetrical and includes out-of-plane rotations of individual bifurcations. For drug deposition purposes, the model was divided into three physical sections, which were the mouth-throat, generations G0–G2 and G3–G5.

The dual flow mouthpiece was designed in house to allow separate streams of nebulized drug aerosol and humidified air to be introduced into the MT-TB geometry (Fig. 1(b)). For this initial mouthpiece prototype, inner and outer diameters were selected to provide equal mean velocities of the aerosol and humidity air streams. During aerosol generation, the total airflow rate (nebulizer + humidified air) in the MT-TB model was 30±2 L/min. Exit flow conditions through the TB model geometry were controlled using individual needle valves located downstream of the model that were connected to an airflow source operating at a total flow rate of 30±2 L/min to match the inlet flow. Division of the outlet flow was set based on the values reported by Horsfield *et al.* (35). The MT-TB model was equilibrated and maintained at a constant temperature and humidity (Espec Environmental Cabinet, Grand Rapids, MI) of 37°C and 99% relative humidity (RH) to ensure that the airway walls within the model were wetted and at equilibrium. Temperature and relative humidity measurements were made using a HUMICAP Handheld Meter (HMP75, Vaisala, Helsinki, Finland).

ECG Aerosol Drug Deposition Studies

In order to investigate *in vitro* aerosol deposition in the realistic MT-TB single path geometry using the ECG technique, separate streams of nebulized albuterol sulfate nano-aerosol droplets (560 and 900 nm MMADs) and saturated humidified air (39°C—ECG, 25°C—control) were combined using the dual flow mouthpiece assembly which was attached to the inlet of the MT-TB model (Fig. 1(a) and (b)). A modified compressed air-driven humidifier system (Vapotherm 2000i, Stevensville, MD) was employed to generate the heated and saturated air that entered the airway model geometry at a flow rate of 20 L/min. Supersaturated conditions were produced when the humidified air stream, which had an inlet relative humidity (RH) of 100%, was mixed with the cooler aerosol stream (21°C). As a result, ECG conditions consisted of a humidified air inlet temperature of 39°C and a temperature difference from the aerosol stream of 18°C, which was theoretically able to produce supersaturation and significant growth. The control case had a humidified air inlet temperature of 25°C, resulting in a temperature differential of 4°C and expected minimal growth. As indicated, the wall temperature was maintained at body conditions (37°C), which may produce some evaporation for the control case. Finally, for comparison with a conventional delivery device that is currently employed clinically, MT-TB model deposition was investigated for a commercially available MDI (Proventil HFA, Key Pharmaceuticals, Kenilworth, NJ). Proventil HFA is a suspension MDI formulation containing albuterol sulfate, oleic acid and ethanol with HFA 134a as the propellant. For this study, five actuations from a single MDI were made into the MT-TB model with an airflow rate of 30 L/min drawn through the geometry. As with the ECG case, the model was held at 37°C and 99% relative humidity (RH).

Following aerosol generation and deposition, the model was disassembled, and wall washings were taken from three regions of the model: the mouth-throat, G0–G2 and G3–G5. Appropriate volumes of water were used to collect albuterol sulfate deposited on the walls of the model. The mean (SD) amount of drug deposited in each section of the model was determined by quantitative HPLC albuterol sulfate analysis of the washings obtained from the surfaces. The deposition fraction results were expressed as a percentage of the total delivered dose of albuterol sulfate. For the ECG and control studies, the mean (SD) total delivered dose was determined in separate experiments using a filter capture apparatus operating at 30 L/min. For the MDI experiment, the label claim dose delivered from the mouthpiece was used for the total delivered dose (108 μg).

CFD Model

A CFD model was implemented that can accurately simulate local temperature and humidity fields, together with droplet trajectories, size change, and deposition within the MT-TB model during the ECG process. Considering the flow field, laminar, transitional, and turbulent conditions are expected. To effectively address this broad range of flow conditions, a low Reynolds number (LRN) k-ω turbulence model was selected. This model has previously been well tested and found to provide good estimates of aerosol transport and deposition in upper airway models (36,37). To evaluate the variable temperature and RH fields in the MT-TB model, interconnected relations governing the transport of heat and mass (water vapor) were also included. These governing equations were previously presented in detail by Longest and Xi (38) and Longest *et al.* (39).

To model droplet trajectories, growth, and deposition, a previously developed and tested combination of a commercial code (Fluent 6.3, ANSYS Inc.) and user functions was implemented. User routines were employed to better model near-wall conditions and to simulate aerosol condensation and evaporation in the complex three-dimensional temperature and humidity fields. Previous studies have shown that the isotropic turbulence approximation, which is assumed with the LRN k-ω model, can over-predict aerosol deposition (40). As a result, a user routine was employed to account for anisotropic near-wall turbulence, as described by Longest *et al.* (39). Other additions to the particle tracking model included (i) a correction to better predict the Brownian motion of submicrometer aerosols and (ii) improved near-wall interpolation of fluid velocities.

A user routine was employed to model interconnected droplet temperature and size change resulting from condensation and evaporation. This droplet model accounts for the Kelvin effect, hygroscopicity arising from the dissolved drug, and the effect of droplet temperature on surface vapor pressure. The effect of the discrete aerosol phase on the continuous heat and water vapor fields was also included in the model, which is referred to as two-way coupling. Experimentally measured concentrations of 1.2×10^5 and 2.8×10^5 particles/cm^3 for the 560 and 900 nm aerosols (after mixing with the humidity stream) were employed to assess the two-way coupling effects.

The CFD model employed in this study has previously been tested in comparison with experimental deposition results. For both constant-sized particles and evaporating droplets, the CFD model was shown to accurately predict local and sectional deposition profiles in comparison with *in vitro* experiments (6,37,41). Good agreement with experimental deposition results has been shown for both nano- and micro-meter aerosols (11,32). Longest and Hindle recently presented a CFD model of ECG in detail (31). In this study, excellent agreement was found between experimental measurements of final particle size after condensational growth and CFD predictions. However, aerosol deposition was not assessed experimentally or with the CFD model. In the current study, *in vitro* deposition results in individual sections of the MT-TB geometry are compared with CFD predictions. Numerical predictions are then used to assess final outlet aerosol size, based on the previous validation study of Longest and Hindle (31). In performing the CFD simulations, previously established best-practices were implemented to provide a high quality solution. All transport equations were discretized to be at least second-order accurate in space and time. The computational mesh was constructed in Gambit 2.2 (ANSYS, Inc.) and consisted entirely of hexahedral control volumes. Previous studies by Longest and Vinchurkar (42) and Vinchurkar and Longest (43) have shown that hexahedral grids provide a better quality solution in aerosol deposition studies compared with tetrahedral and hybrid configurations. Convergence of the flow field solution was assumed when the global mass residual had been reduced from its original value by five orders of magnitude and when the residual reduction rates for both mass and momentum were sufficiently small. To improve accuracy and to better resolve the significant change in flow scales during deposition, all calculations were performed in double precision. For the MT-TB model, grid convergent results were found to occur with meshes consisting of approximately 850,000 control volumes. In order to produce convergent deposition results for all droplet sizes considered, groups of 3,000 droplets were released to represent each of the 9 size bins considered, resulting in 27,000 tracked elements. The final mass deposition results were scaled to reflect the experimentally determined initial aerosol size distribution for comparison with the measured deposition fractions of drug mass. Doubling the number of droplets considered had a negligible impact on both total and sectional deposition results.

RESULTS AND DISCUSSION

ECG Aerosol Drug Deposition Studies

Table I shows the *in vitro* regional drug deposition of the 560 and 900 nm albuterol sulfate aerosols when inhaled through the MT-TB model with humidified air under ECG (39°C) and control (25°C) conditions. Total drug deposition within the MT-TB model significantly increased for both the 560 and 900 nm aerosols when delivered using ECG conditions compared to the control. The mean (SD) total deposition in the MT-TB model increased from 3.3 (1.1) % for control studies to 6.5 (1.5) % ($P<0.05$; t-test) for the ECG case with the 560 nm aerosol. Similar values for the 900 nm aerosol were 2.2 (0.7) and 7.8 (0.5) %, respectively ($P<0.05$; t-test). In addition to considering the overall total deposition, it is important to consider the regional deposition within the MT-TB model. For both the ECG and control conditions, MT drug deposition was low for these nano-aerosols (Table I). These results agree with the literature observations that suggest nano-aerosols (>10 nm) are readily able to penetrate the MT region (11,12). Using the same MT-TB geometry with a conventional pharmaceutical inhaler, the MT deposition was observed to be significantly higher. For the MDI (Proventil HFA), the mean (SD) albuterol sulfate deposition in the MT-TB model was found to be 49.7 (7.2)% of the dose. The majority of the dose from the MDI was deposited in the MT region (46.0%), with only 3% and 0.6% deposited in the G0–G2 and G3–G5 regions, respectively. Similar

deposition results have been observed in the literature using a dry powder inhaler. For example, Byron *et al.* (44) used the same MT geometry to observe aerosol deposition from the Novolizer DPI (45) as a function of inspiratory flow patterns. They reported 50–60% albuterol deposition in the MT region following actuation of the DPI using 6 different individual inhalation profiles.

The introduction of the ECG conditions did not significantly increase the deposition in the MT region for the 560 nm aerosol (difference of 0.2%), while there was only a small (1.5%) but significant increase for the 900 nm aerosol. This is an important observation, as our previous studies with a condensational growth tube indicated that using the ECG conditions produced rapid and continued growth (27). This previous study indicated that growth to particle sizes of 1–3 μm with ECG occurred during a residence time of approximately 200 ms in a condensation growth tube (27). This is equivalent to the time it takes an aerosol droplet to travel from the mouth to the first bifurcation at a flow rate of 30 L/min. Using the realistic MT geometry, any growth that did occur during this initial transit through the MT region did not drastically alter the aerosol deposition in the MT. However, aerosol growth with the ECG conditions did significantly increase the albuterol sulfate deposition in the TB regions, G0–G2 and G3–G5, of the airway model compared to the control (25°C) for both nano-aerosols ($P<0.01$; t-test). Table I reveals that the albuterol sulfate deposition fraction ratio comparing ECG to control increased as the aerosol penetrated further into the model geometry. A progressive increase in the deposition fraction for ECG compared to the control conditions indicates that the aerosol is increasing in size, resulting in more inertial impaction.

Table I Mean (SD) Regional Deposition of Albuterol Sulfate in the MT-TB Airway Model

MT-TB Model Region	Deposition Fraction Control (25°C)	Deposition Fraction ECG (39°C)	Deposition Fraction Ratio (ECG/Control)
560 nm Nano-Aerosol			
MT	1.8 (0.9)%	2.0 (0.6)%	1.1
G0-G2	1.1 (0.3)%	2.9 (0.6)%	2.6
G3-G5	0.3 (0.4)%	1.7 (0.7)%	5.7
900 nm Nano-Aerosol			
MT	0.8 (0.2)%	2.3 (0.4)%	2.9
G0-G2	1.2 (0.6)%	4.0 (0.3)%	3.3
G3-G5	0.2 (0.1)%	1.4 (0.4)%	7
Proventil HFA MDI			
MT	46.0 (7.2)%	–	–
G0-G2	3.0 (0.4)%	–	–
G3-G5	0.6 (0.2)%	–	–

It is well known that hygroscopic aerosols increase in size due to water vapor condensation in the warm, humid, subsaturated respiratory airways (23–26). However, the size increase of submicrometer aerosols at an *in vivo* relative humidity of 99.5% is insufficient to largely increase lung retention for most aerosols, as evidenced by the significant exhaled fraction. A number of mathematical models have been formulated for the hygroscopic growth of respiratory aerosols at RH values below 100% (23,24,46–48). The hygroscopic growth of most pharmaceutical aerosols result in size increases of less than 100% at RH values of 99.5% and below, which would be insufficient to facilitate the growth required for the nano-aerosols used in this study. Zhang *et al.* (49) developed a CFD model of hygroscopic growth in the upper respiratory tract. It was found that saline concentrations of 10% and higher were required for hygroscopic growth to have a significant impact on deposition. The newly proposed ECG platform combines (i) a controlled inhalable water vapor humidity source with (ii) a nano-aerosol generation and delivery device. The humidity source is used to create a controlled supersaturated environment within general regions of the lung. The aerosol has a size that can effectively penetrate the mouth-throat (MT), and, as it reaches the TB region, the droplets will increase in size due to enhanced condensational growth in the controlled supersaturated environment. As a result, small aerosols can be effectively delivered past the MT and into the deep lung or a specific TB region.

These *in vitro* experimental results have demonstrated, first, the changes in nano-aerosol drug deposition within a realistic MT-TB geometry when using the enhanced condensational growth platform. This approach appears to offer a suitable method of delivering nano-aerosols through the extrathoracic region, with minimal deposition, to the tracheobronchial airways and beyond. Aerosol deposition and nearly full lung retention would then be possible as enhanced condensational growth increases the droplet size. Second, they can be used to validate the predictions of the developed *in silico* CFD model for the ECG process in the MT-TB geometry. The CFD model is then used to further probe and elucidate the aerosol transport phenomena as the nano-aerosols flow through the simulated respiratory airways.

CFD Modeling

The utility of the CFD model is that it is able to accurately simulate local temperature and humidity fields, droplet trajectories, condensation and evaporation, and two-way coupling between the continuous and discrete phases. In this study, CFD simulations of the ECG process have been adapted to model the aerosol transport and growth taking place within the MT-TB model. Fig. 2 shows the relative

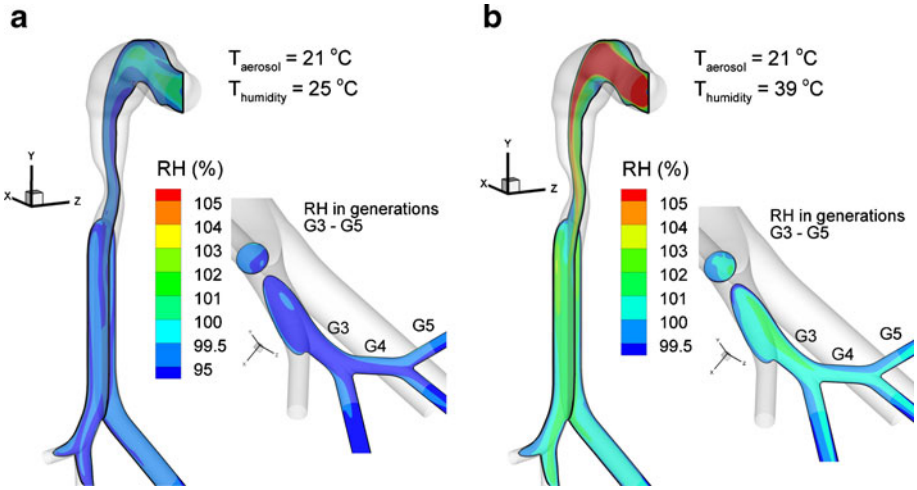

Fig. 2 Predicted relative humidity (RH) conditions for the **a** control ($T_{aerosol}$ = 21°C and $T_{humidity}$ = 25°C) and **b** ECG ($T_{aerosol}$ = 21°C and $T_{humidity}$ = 39°C) conditions.

humidity fields for the control and ECG cases within the airway model. Subsaturated conditions dominate for the control case as a result of the nebulized aerosol and humidified air having a lower temperature than the wall temperature of the airway model, which is maintained at 37°C. In contrast, supersaturated conditions were evident for the ECG conditions as the saturated air is cooled by the airway wall and as it mixes with the nebulized aerosol. Under these steady-state conditions, supersaturation was still present in generations G3–G5 of the TB model.

Fig. 3 shows the predicted droplet trajectories for the nano-aerosol with an initial diameter of 560 nm. In this simulation, 200 monodisperse droplets with a diameter of 560 nm were initiated in the model to visualize size change of the aerosol. Little growth was observed for the control experiment as the aerosol particles flowed through the MT-TB model under saturated conditions. In contrast, for the ECG conditions, the aerosol size increased from 560 nm to greater than 3 μm in the TB region. This agrees well with previous *in vitro* and CFD studies that were performed using a simple, shorter condensational growth tube and an aerosol with a mean MMAD of 560 nm (31). In those studies, under ECG conditions, the final experimental particle size following growth was 2.7 μm, and the CFD-predicted size was 2.6 μm. For the control study at 25°C also performed using the growth tube, similar experimental and CFD predicted final sizes were 610 nm and 590 nm, respectively.

For the previous studies using the condensational growth tube, it was relatively simple to measure the final particle size distribution of the aerosol as it exits the tube using cascade impaction (27,31). However, in the current study, due to the bifurcating TB model that was employed, measurement of the final particle size after passage through the airways proved more challenging; therefore, CFD-predicted sizes were used. In part, this was due to the

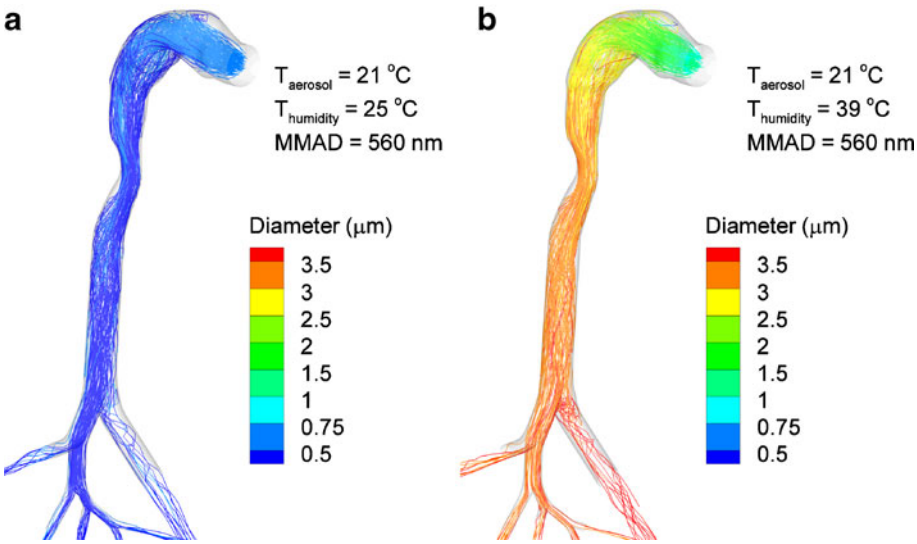

Fig. 3 Predicted droplet trajectories contoured according to diameter for the **a** control ($T_{aerosol}$ = 21°C and $T_{humidity}$ = 25°C) and **b** ECG ($T_{aerosol}$ = 21°C and $T_{humidity}$ = 39°C) conditions.

dilution effects as the aerosol is sequentially split into the different airways generations. In contrast, the CFD model can readily predict the polydisperse aerosol distribution at multiple sites in the flow field and calculate resulting MMADs. Fig. 4 shows the experimentally measured initial particle size distributions compared to the CFD predictions as the aerosol exits the MT region and at the exit of the G5 bronchi for the 560 nm and 900 nm aerosols. For the 560 nm aerosol, the CFD model predicted a significant increase in the aerosol size (3.1 μm) as it exits the MT region under the ECG conditions. Similar growth was observed for the 900 nm aerosol at the exit of the MT region (3.6 μm). For the 560 nm aerosol, this growth was observed to continue during passage through to the G5 bronchi reaching a size of 3.6 μm; however, for the 900 nm aerosol, less change was observed after it exited the G5 bronchi (3.9 μm) in terms of MMAD.

A comparison of the numerically predicted and experimentally determined localized deposition fractions are presented in Fig. 5 for the 560 nm aerosol. Deposition in the control and ECG studies is shown as a function of droplet size in the MT-TB model, and the *in vitro* and *in silico* deposition fractions are compared. On a sectional basis (MT, G0-G2 and G3-G5) and overall, the CFD model results of deposition fraction provide good agreement with the experimental results. In addition, the CFD model provides further insight into the fate of the aerosol as it is transported through the MT-TB model. In both the control and ECG experiments, the main site of deposition in the MT region appeared to be around the larynx. This region was a deposition site for both the control aerosol, which had not changed in its original size, and the ECG aerosol, which had increased in size to 2–4 μm. Both the CFD model and the experimental results showed a significant increase in aerosol deposition in the G3-G5 region for the ECG conditions compared to the control, which was indicative of the aerosol size increase.

Fig. 6(a–d) compares the CFD-predicted regional MT-TB model drug deposition fractions to those obtained in the *in vitro* experimental studies. The CFD model produced good agreement with the experimental results and was predictive of the major trends that were observed. On a sectional basis, the CFD predictions matched the *in vitro* results reasonably well with the predictions falling inside the SD error bar ranges in most cases. Possible sources of error may arise due to a number of experimental factors, including minor liquid flow on the wet airway walls altering the final recovery site of deposited aerosol. Comparing the CFD predictions to the experimental data, the % relative errors for the total deposition fraction of the 560 nm aerosol were 33% for control and 13.8% for ECG. Similar values for the 900 nm aerosol were 24% and 2.6%, respectively. For all the cases considered, the predicted total deposition results were within the SD error bars of the *in vitro* experiments.

These studies have demonstrated that in a realistic *in vitro* airway model, it is feasible to deliver a nano-aerosol in such a way that deposition in the MT region of the airway is minimized compared to conventional MDI and DPI inhalers. By using the ECG platform for both the 560 and 900 nm aerosols, deposition in the MT region was low and was then followed by increased deposition in the G0–G5 regions of the airway geometry as the aerosol particle size increased due to condensational growth. These results were for a single set of condensational growth conditions; however, using the CFD model, we are able to efficiently investigate the effects of changing the inlet aerosol conditions on the ECG process. Fig. 7 shows a

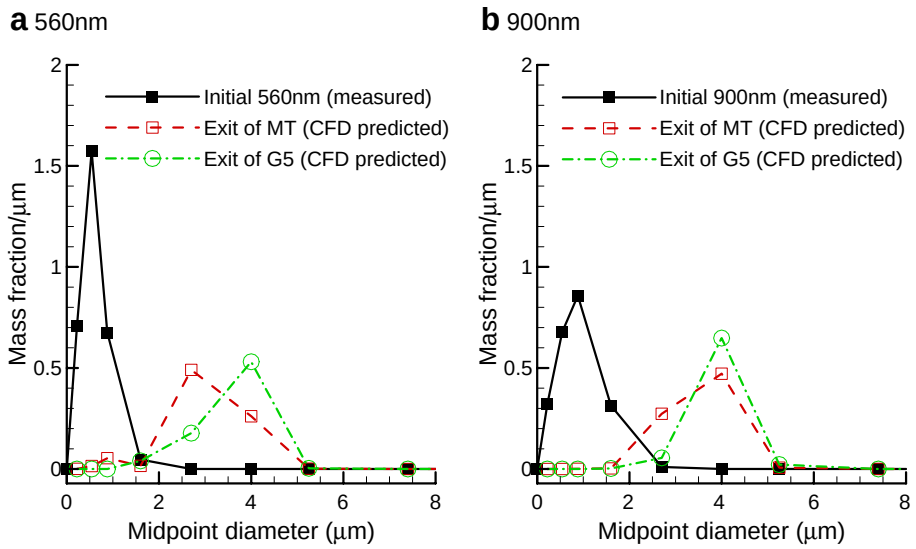

Fig. 4 Initial (*in vitro* measured) and CFD predictions of exiting polydisperse size distributions for the **a** 560 nm and **b** 900 nm aerosols.

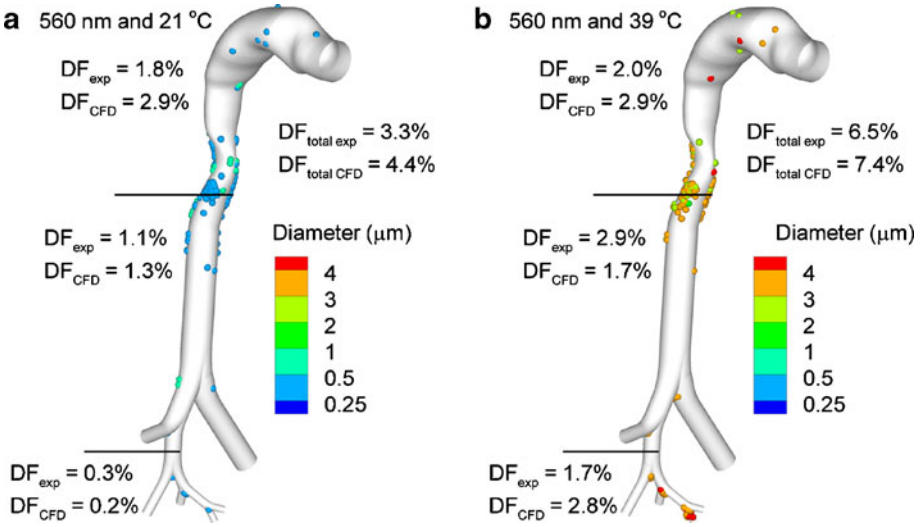

Fig. 5 Deposition locations and deposition fractions (DF) of drug mass for an initially 560 nm aerosol and **a** control ($T_{aerosol} = 21°C$ and $T_{humidity} = 25°C$) *vs.* **b** ECG ($T_{aerosol} = 21°C$ and $T_{humidity} = 39°C$) conditions. Numerically predicted and experimentally determined deposition fractions are shown for each section considered.

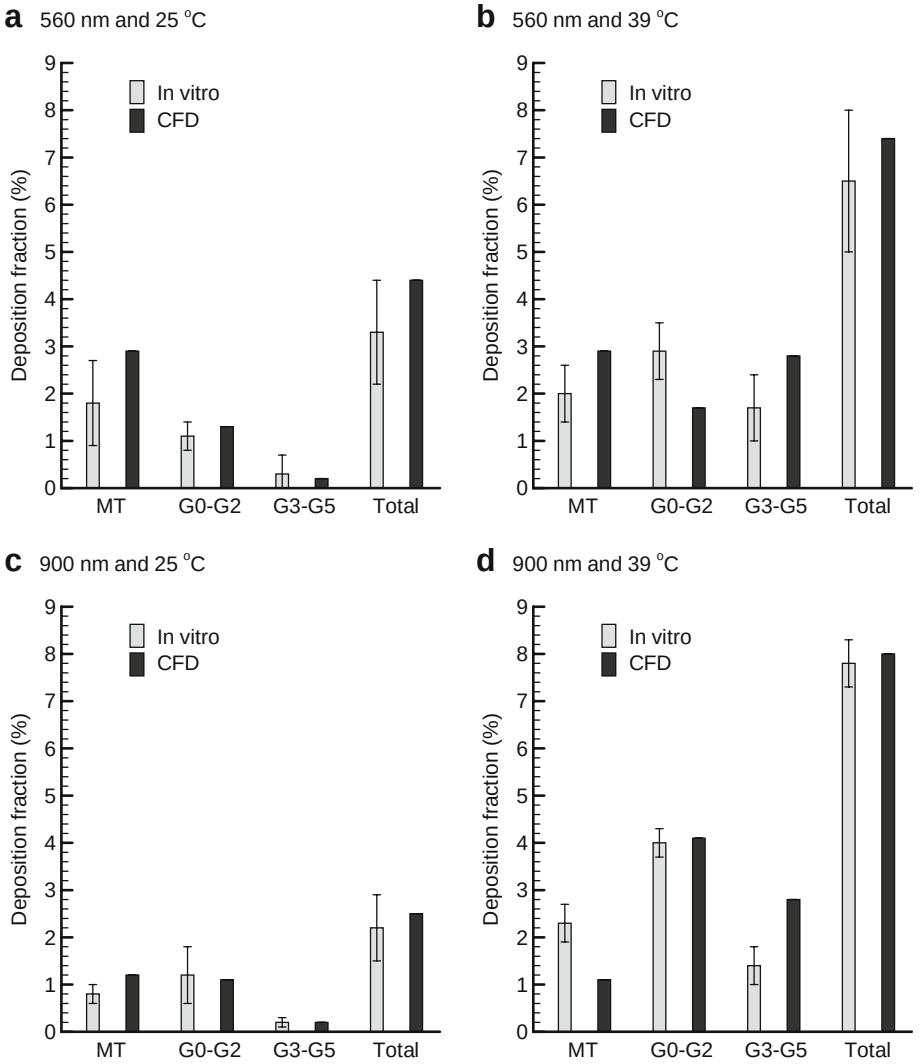

Fig. 6 Comparison of *in vitro vs.* CFD-predicted deposition fractions (DF) of drug mass on a sectional basis for **a** $MMAD_{initial} = 560$ nm and $T_{humidity} = 25°C$, **b** $MMAD_{initial} = 560$ nm and $T_{humidity} = 39°C$ (ECG), **c** $MMAD_{initial} = 900$ nm and $T_{humidity} = 25°C$, and **d** $MMAD_{initial} = 900$ nm and $T_{humidity} = 39°C$ (ECG). The aerosol inlet temperature was 21°C in all cases. The error bars denote +/− one standard deviation.

case study of how it may be possible to further optimize the ECG process using different inlet conditions. In this example, both the 900 nm aerosol and humidity were supplied at 39°C, and the airway walls were maintained at 37°C. Fig. 7(a) shows that the development of supersaturated conditions appears delayed within the mouth region and therefore has a more gradual onset as the aerosol enters the model. For this inhalation condition, the wall temperature cools the airstream and produces a more evenly distributed supersaturation environment which extends deeper into the airway. Fig. 7(b) shows that the particle trajectories exhibit a more gradual increase in size which corresponds with the supersaturation within the model. The MMAD of the aerosol exiting the MT was predicted to be 2.8 μm, and continued condensational growth was observed with the aerosol exiting G5 with a predicted size of 3.4 μm (Fig. 7(c)). These conditions produced an altered growth profile compared to the ECG conditions described in Fig. 4 for the 900 nm aerosol, which had a larger particle size (3.1 μm) exiting the MT region and slower growth as the droplets passed through to G5. Finally, Fig. 7(d) shows a comparison of predicted % aerosol deposition fractions for the control and ECG conditions that were applied previously in this paper with the optimized ECG conditions (39°C for both aerosol and humidified air). The optimized conditions appear to produce a progressively increasing deposition fraction as the nano-aerosol penetrates into the airway model. This is achieved by decreasing the deposition in the G0–G2 region compared with the original ECG conditions. From a delivery perspective, increasing deposition as the aerosol penetrates deeper within the lungs may be advantageous for maintaining a constant or increasing deposited drug dose per unit surface area.

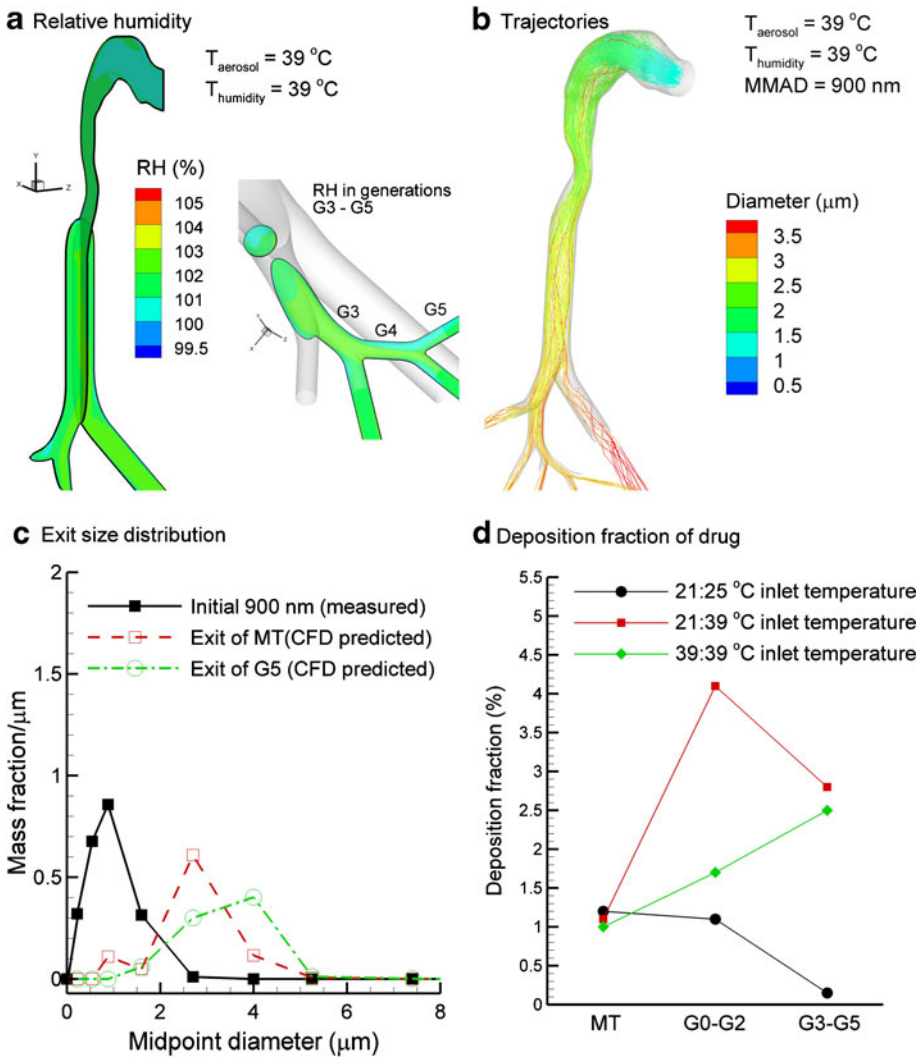

Fig. 7 CFD results of an improved inlet condition with the aerosol and humidity temperatures both at 39°C for the 900 nm aerosol, presented as **a** the relative humidity field, **b** droplet trajectories, **c** exiting size distributions, and **d** deposition fraction of drug.

CONCLUSIONS

This study illustrated the potential utility of the ECG methodology for the delivery of nano-aerosols with high efficiency to the respiratory airways with minimal extra-thoracic deposition. The ECG platform may offer significant flexibility in the resulting deposition profile following passage through the mouth-throat region by controlling the rate and extent of aerosol growth. This may allow targeting of deposition sites within the airways. Future studies will investigate the effects of the physio-chemical drug properties and realistic inhalation profiles on ECG growth characteristics. Evaluation of continued growth in deeper lung generations is also of interest.

ACKNOWLEDGEMENTS

This study was supported by Award Number R21HL094991 from the National Heart, Lung, And Blood Institute. The content is solely the responsibility of the authors and does not necessarily represent the official views of the National Heart, Lung, And Blood Institute or the National Institutes of Health.

REFERENCES

1. Borgstrom L, Olsson B, Thorsson L. Degree of throat deposition can explain the variability in lung deposition of inhaled drugs. J Aerosol Med. 2006;19:473–83.
2. Newman SP. A comparison of lung deposition patterns between different asthma inhalers. J Aerosol Med. 1995;8 Suppl 3:S21–26. discussion S27.
3. Leach CL, Davidson PJ, Bouhuys A. Improved airway targeting with the CFC-free HFA-beclomethasone metered-dose inhaler compared with CFC-beclomethasone. Eur Respir J. 1998;12: 1346–53.
4. Smaldone GC. Advances in aerosols: adult respiratory disease. J Aerosol Med. 2006;19:36–46.
5. Byron PR. Drug delivery devices: issues in drug development. Proc Am Thorac Soc. 2004;1:321–8.
6. Longest PW, Hindle M, Das Choudhuri S, Byron PR. Developing a better understanding of spray system design using a combination of CFD modeling and experiment. In: Dalby RN *et al.*, editors. Proceedings of Respiratory Drug Delivery 2008. Illinois: Davis Healthcare International; 2008. p. 151–63.
7. Hindle, M. Soft mist inhalers: a review of current technology. The Drug Delivery Companies Report Autumn/Winter. 2004;31–4.
8. Cheng YS, Fu CS, Yazzie D, Zhou Y. Respiratory deposition patterns of salbutamol pMDI with CFC and HFA-134a formulations in a human airway replica. J Aerosol Med. 2001;14:255–66.
9. Longest PW, Hindle M, Das Choudhuri S, Xi J. Comparison of ambient and spray aerosol deposition in a standard induction port and more realistic mouth–throat geometry. J Aerosol Sci. 2008;39:572–91.
10. Zhang Y, Gilbertson K, Finlay WH. *In vivo-in vitro* comparison of deposition in three mouth-throat models with Qvar and Turbuhaler inhalers. J Aerosol Med. 2007;20:227–35.
11. Xi J, Longest PW. Effects of oral airway geometry characteristics on the diffusional deposition of inhaled nanoparticles. ASME J Biomech Eng. 2008;130:011008.
12. Cheng YS. Aerosol deposition in the extrathoracic region. Aerosol Sci Tech. 2003;37:659–71.
13. Card JW, Zeldin DC, Bonner JC, Nestmann ER. Pulmonary applications and toxicity of engineered nanoparticles. Am J Physiol Lung Cell Mol Physiol. 2008;295:L400–411.
14. Sung JC, Pulliam BL, Edwards DA. Nanoparticles for drug delivery to the lungs. Trends Biotechnol. 2007;25:563–70.
15. Cohen BS, Sussman RG, Lippmann M. Ultrafine particle deposition in a human tracheobronchial cast. Aerosol Sci Tech. 1990;12:1082–93.
16. Jaques PA, Kim CS. Measurement of total lung deposition of inhaled ultrafine particles in healthy men and women. Inhal Toxicol. 2000;12:715–31.
17. Morawska L, Hofmann W, Hitchins-Loveday J, Swanson C, Mengersen K. Experimental study of the deposition of combustion aerosols in the human respiratory tract. J Aerosol Sci. 2005; 36:939–57.
18. Stahlhofen W, Rudolf G, James AC. Intercomparison of experimental regional aerosol deposition data. J Aerosol Med. 1989;2:285–308.
19. Pandey R *et al.* Poly (DL-lactide-co-glycolide) nanoparticle-based inhalable sustained drug delivery system for experimental tuberculosis. J Antimicrob Chemother. 2003;52:981–6.
20. Dickinson PA, Howells SW, Kellaway IW. Novel nanoparticles for pulmonary drug administration. J Drug Target. 2001;9:295–302.
21. Azarmi S, Roa WH, Lobenberg R. Targeted delivery of nanoparticles for the treatment of lung diseases. Adv Drug Deliv Rev. 2008;60:863–75.
22. Nyambura BK, Kellaway IW, Taylor KMG. Insulin nanoparticles: stability and aerosolization from pressurized metered dose inhalers. Int J Pharm. 2009;375:114–22.
23. Ferron GA. The size of soluable aerosol particles as a function of the humidity of the air: application to the human respiratory tract. J Aerosol Sci. 1977;3:251–67.
24. Ferron GA, Oberdorster G, Hennenberg R. Estimation of the deposition of aerosolised drugs in the human respiratory tract due to hygroscopic growth. J Aerosol Med. 1989;2:271.
25. Finlay WH. Estimating the type of hygroscopic behavior exhibited by aqueous droplets. J Aerosol Med. 1998;11:221–9.
26. Martonen TB, Bell KA, Phalen RF, Wilson AF, Ho A. Growth rate measurements and deposition modeling of hygroscopic aerosols in human tracheobronchial models. In: Walton WH, editor. Inhaled particles V. Oxford: Pergamon; 1982. p. 93–107.
27. Longest PW, McLeskey JT, Hindle M. Characterization of nanoaerosol size change during enhanced condensational growth. Aerosol Sci Tech. 2010;44:473–483.
28. Longest PW, Hindle M, Xi J. Effective delivery of nanoparticles and micrometer-sized pharmaceutical aerosols to the lung through enhanced condensational growth. International Patent Application PCT/US2009/034360: 2009.
29. Hinds WC. Aerosol technology: properties, behavior, and measurement of airborne particles. New York: Wiley; 1999.
30. Friedlander SK, Windeler RS, Weber AP. Ultrafine particle formation by aerosol processes in turbulent jets: mechanisms and scale-up. NanoStruct Mat. 1994;4:521–8.
31. Longest PW, Hindle M. CFD simulations of enhanced condensational growth (ECG) applied to respiratory drug delivery with comparisons to *in vitro* data. J Aerosol Sci. 2010. doi:10.1016/j.jaerosci.2010.04.006.
32. Xi J, Longest PW. Transport and deposition of micro-aerosols in realistic and simplified models of the oral airway. Ann Biomed Eng. 2007;35:560–81.

33. Heistracher T, Hofmann W. Physiologically realistic models of bronchial airway bifurcations. J Aerosol Sci. 1995;26:497–509.
34. Yeh HC, Schum GM. Models of human lung airways and their application to inhaled particle deposition. Bull Math Biol. 1980;42:461–80.
35. Horsfield K, Dart G, Olson DE, Cumming G. Models of the human bronchial tree. J Appl Physiol. 1971;31:207–17.
36. Longest PW, Hindle M. Evaluation of the respimat soft mist inhaler using a concurrent CFD and *in vitro* approach. J Aerosol Med. 2009;22:99–112.
37. Longest PW, Hindle M, Das Choudhuri S. Effects of generation time on spray aerosol transport and deposition in models of the mouth-throat geometry. J Aerosol Med. 2009;22:67–84.
38. Longest PW, Xi J. Condensational growth may contribute to the enhanced deposition of cigarette smoke particles in the upper respiratory tract. Aerosol Sci Tech. 2008;42:579–602.
39. Longest PW, Hindle M, Das Choudhuri S, Byron PR. Numerical simulations of capillary aerosol generation: CFD model development and comparisons with experimental data. Aerosol Sci Tech. 2007;41: 952–73.
40. Matida EA, Finlay WH, Grgic LB. Improved numerical simulation of aerosol deposition in an idealized mouth-throat. J Aerosol Sci. 2004;35:1–19.
41. Xi J, Longest PW, Martonen TB. Effects of the laryngeal jet on nano- and microparticle transport and deposition in an approximate model of the upper tracheobronchial airways. J Appl Physiol. 2008;104:1761–77.
42. Longest PW, Vinchurkar S. Effects of mesh style and grid convergence on particle deposition in bifurcating airway models with comparisons to experimental data. Med Eng Phys. 2007;29: 350–66.
43. Vinchurkar S, Longest PW. Evaluation of hexahedral, prismatic and hybrid mesh styles for simulating respiratory aerosol dynamics. Comput Fluids. 2008;37:317–31.
44. Byron PR, Delvadia RR, Longest PW, Hindle M. Stepping into the Trachea with Realistic Physical Models: Uncertainties in Regional Drug Deposition from Powder Inhalers. In: Dalby, RN *et al.*,editors. Respiratory Drug Delivery 2010. Illinois: Davis Healthcare International Publishing; 2010. (in press).
45. Kohler D. The Novolizer: overcoming inherent problems of dry powder inhalers. Respir Med. 2004;98(Suppl A):S17–21.
46. Ferron GA, Kreyling WG, Haider B. Inhalation of salt aerosol particles - II. Growth and deposition in the human respiratory tract. J Aerosol Sci. 1988;19:611–31.
47. Robinson R, Yu CP. Theoretical analysis of hygroscopic growth rate of mainstream and sidestream cigarette smoke particles in the human respiratory tract. Aerosol Sci Tech. 1998;28: 21–32.
48. Finlay WH, Stapleton KW. The effect on regional lung deposition of coupled heat and mass-transfer between hygroscopic droplets and their surrounding phase. J Aerosol Sci. 1995;26:655–70.
49. Zhang Z, Kleinstreuer C, Kim CS. Isotonic and hypertonic saline droplet deposition in a human upper airway model. J Aerosol Med. 2006;19:184–98.